Roles of Conformational Flexibility in the

Crystallization of Stereo-Irregular Polymer

Navin Kafle,[†] Yuta Makita,[†] Ying Zheng,^{†, |}Derek Schwarz,[†] Hiromichi Kurosu, [|] Pengju Pan, [|] James M. Eagan, [†] Yuki Nakama, [‡] Shigetaka Hayano, [‡] and Toshikazu Miyoshi ^{†, *}

†School of Polymer Science and Polymer Engineering, The University of Akron, Akron, Ohio 44325-3909, United States. ‡Zeon Corporation R&D Center, 1-2-1 Yako, Kawasaki-ward, Kawasaki City, Kanagawa 210-9507, Japan. |State Key Laboratory of Chemical Engineering, College of Biological and Chemical Engineering, Zhejiang University, 38 Zheda Road, Hangzhou 310027, China. || Department of Clothing Environmental Science, Nara Women's University, Kitauoya, Higashimachi, Nara 630-8506, Japan.

ABSTRACT Stereo-regularity significantly influences the crystallization, mechanical and thermal properties of polymers. In this work, we investigate crystallization behaviors and molecular dynamics of *atactic* (*a*)-, *isotactic* (*i*)-, and *syndiotactic* (*s*)-hydrogenated Poly(norbornene) (hPNB)s by using small angle X-ray scattering (SAXS) and solid-state (ss) NMR. *a*-hPNB exhibits a much higher crystallinity (Φ_c) (82%) and Long period (*L*) (80 nm) than *i*- and *s*-hPNB (50–55% and 17–21 nm). Moreover, in the *s*-hPNB crystalline region, chain dynamics are not thermally activated up to the melting temperature (T_m) while in the crystalline regions of *i*- and *a*-hPNB, small amplitude motions occur in a slow dynamic regime of 10^{-2} – 10^2 s. The molecular dynamics follows Arrhenius behavior in *a*-hPNB up to crystal-crystal transition temperature (T_{cc}), while these dynamics are surprisingly saturated in *i*-hPNB under these conditions. Temperature dependence of the molecular dynamics leads to different crystal-crystal transitions between *i*- and *a*-hPNBs: *i*-hPNB changes *trans* conformation to *gauche* one due to

the localized bond rotations where chain dynamics are restricted, whereas *a*-hPNB keeps a nearly *trans* conformation and conducts fast chain dynamics due to the amplified C-C bond rotations in the high temperature phase. Such fast chain dynamics leads to unique crystallization behaviors of hPNB, specifically in *atactic*-configuration due to configurational disorder coupled with conformational flexibility (CDCF).

1. INTRODUCTION

Weaving macroscopic properties with hierarchical structure into semicrystalline polymers is one of ultimate goals for polymer science. In ideal cases, polymer crystals possess three-dimensional long-range order; however, with most polymer crystals containing physical and/or chemical disorder, ¹⁻⁴ degrees of crystal order as well as mechanical and thermal properties lessen. On the other hand, some polymer crystals benefit from this disorder, leading to structural evolutions and improvements in the properties of semicrystalline polymers. ⁵⁻⁸ Examples of such cases include the following: polyethylene (PE) which under high pressure and high temperature forms extended chain crystal (ECC)s, ^{5,6} 1,4 *trans*-polybutadiene (1,4-*t*PBD) which experiences a sudden increase in lamellae thickness in the high temperature phase, ⁷ and poly(tetrafluoroethylene) (PTFE) which shows extremely high orientation at high temperature. ⁸ In these cases, phase transition commonly induces rotational disorder which accompanies fast and anisotropic chain dynamics concomitant with translation along the chain axis. ⁹⁻¹²Such anisotropic and rapid chain dynamics are the genesis for unusual structure evolutions of semicrystalline polymers. ⁵⁻⁸

Stereoregularity is a crucial element in polymer chemistry because of its immense impact on crystalline order, $^{12, 13}$ lamellae thickness, 14 $T_{\rm m}$, 14 and mechanical properties. 15 Lowering stereoregularity leads to imperfection in polymer crystals, 13 with random configurations adopting non-crystalline or low crystalline states. $^{16-18}$ With regards to the effect configuration traditionally has on solid structures, we will present an opposite scenario: A stereo-irregular polymer with higher crystallinity and larger long-

period compared to the stereo-regular counterparts. Given previous examples, it is clear that fast and anisotropic chain dynamics coupled with structural disorder is critical to enhancing crystallinity,⁵⁻⁷ lamellae thickness, 5-7 and molecular orientation. 8 Here, a novel structural disorder of "configurational" disorder coupled with conformational flexibility (CDCF)" is proposed. The idea is grounded on incorporating a flexible unit within the polymer backbone. To this end, we will focus on plastic crystals such as adamantane, 19 cyclohexane, 20 cyclopentane, 21,22 fullerene, 23, 24 etc, which experience some rotation of freedom in the crystalline state. Specifically, cyclopentane and cyclohexane adopt non-planer (puckered) rings and thus gain additionally conformational flexibility (C-C bond rotation) in the solid phase. 20-24 Previously, cyclopentane rings have been successively embedded in a polymer backbone. 25-28 atactic-hydrogenated Poly(norbonene) (a-hPNB) was synthesized via hydrogenation of PNB samples.²⁶ Interestingly, a-hPNB can crystallize efficiently (76%) into a monoclinic lattice with a = 6.94, b = 9.60, c = 12.42 Å, $\beta = 130.7^{\circ}$ and $\rho = 1.019$ g/cm³. This crystal experiences crystal-crystal transition into the monoclinic lattice without lateral order at crystal-crystal transition temperature ($T_{\rm cc}$) of 105 °C²⁶ and long-period (L) reaches ~ 90 nm by annealing above $T_{\rm cc}$. Building on this discovery, isotactic (i)- and syndiotactic (s)-hPNBs were recently synthesized with meso (m) of 100% and racemo (r) of 90%. respectively, at the diad level.²⁹ A set of s-, i-, and a-hPNBs may be an ideal system to identify the importance of CDCF in the crystallization of semicrystalline polymers.

In this work, we investigate the crystallization process for s-, i-, and a-hPNBs via solid-state (ss) NMR spectroscopy and Small Angle X-ray Scattering (SAXS). First, we will demonstrate that the *atactic*-polymer contains a substantially higher degree of crystallinity and greater long period than comparable stereo-regular ones. Secondly, the molecular dynamics of hPNBs at the atomic scale are probed by ssNMR. These results reveal that the cyclopentyl groups within s-hPNB do not conduct slow dynamics up to $T_{\rm m}$, whereas the cyclopentyl groups within a- and i-hPNBs conduct slow molecular dynamics in the crystalline region below crystal-crystal transition temperature ($T_{\rm cc}$). These slow

dynamics trigger phase transitions differently for the two polymers: a-hPNB undergoes fast chain dynamics in the crystalline region above T_{cc} , while i-hPNB induces conformational change above T_{cc} . Finally, we will discuss how CDCF results in unusual crystallization behavior for a-hPNB. Molecular weight and configuration of hPNB used in this study are listed in **Table 1**. Further details regarding polymerization and samples are described in the following section.

Table 1. Molecular weight, configuration, and thermal properties of s-, i-, and a-hPNBs.

	$M_{\rm n}$	Đ	Configuration	$T_{ m m}$	$T_{\rm cc}$	$\Phi_{ m c}$
	(kg/mol)	$(M_{\rm w}/M_{\rm n})$		(°C)	(°C)	(%)
s-hPNB	46	2.2	m:r=10:90	135	None	55
i-hPNB	34	5.2	m:r=100:0	178	150 ^a /None ^b	50
a-hPNB	134	1.9	m:r = 53:47	145	117 ^a /106 ^b	82

a) T_{cc} determined in heating process with a heating rate of 10 °C/min.

2. EXPERIMENTAL SECTION

2.1. Polymer Preparation

Atactic poly(norbornene) (a-PNB): A cyclohexane solution of NB (7.50g, 79.7mmol) and 1-octene (6.3mg, 0.056mmol) was added to toluene solution of (1,3-bis(2,4,6-trimethylphenyl)-2-imidazolidinylidene) dichloro(benzylidene)(tricyclohexylphosphine)ruthenium (1.35 mg, 1.594 μ mol) at 20 °C. After stirring the reaction for 3 hours, the polymerization was quenched with a small amount of ethyl vinyl ether. The resulting polymer was precipitated from ethanol and dried in vacuum at 40 °C for 24 h. a-PNB was obtained quantitatively: $M_n = 134,000$; $M_w/M_n = 1.8$.²⁹

Atactic hydrogenated poly(norbornene) (a-hPNB): A p-xylene solution of a-PNB and a p-xylene solution of 4 equiv. of p-Tos-NHNH₂ were mixed in a glass flask equipped with a three-way stopcock.

b) T_{cc} determined in cooling process with a cooling rate of 10 °C/min.

The mixture was allowed to heat up to the reaction temperature while stirring. Chemical transfer hydrogenation was carried out at 125 °C for 5 h. After the hydrogenation reaction, the obtained polymer was precipitated immediately from ethanol. The precipitation was conducted three times repeatedly to purify the obtained hydrogenated polymer. After purification it was dried at 40 °C for 24 h under vacuum. a-hPNB was obtained quantitatively; meso/racemo = 53/47 and cis/trans = 100:0.²⁹ Syndiotactic poly(norbornene) (s-PNB): A toluene solution of W(=NPh) Cl₄·Et₂O (0.0278 g, 56.7 µmol) (green solution) was mixed with three equivalents of Et₂Al(OEt) at room temperature and stirred. The catalyst mixture was aged at room temperature for an additional 15 min, resulting in a light brown solution. A cyclohexane solution of NB (7.50 g, 79.7 mmol) and 1-octene (0.180 g, 1,59 mmol) was added to the catalyst mixture at 50 °C. After stirring the reaction for 3 hours, the polymerization was quenched with a small amount of ethanol. The obtained polymer was precipitated from ethanol and dried under vacuum at 40 °C for 24 h. s-hPNB was obtained quantitatively: M_n = 46,000 g/mol, M_w/M_n = 2.2 by GPC.²⁹

Syndiotactic hydrogenated poly(norbornene) (s-hPNB): p-xylene solution of s-PNB and a p-xylene solution of 4 equiv. of p-Tos-NHNH₂ were mixed in a glass flask equipped with a three-way stopcock. The mixture was allowed to heat up to the reaction temperature while stirring. Chemical transfer hydrogenation was carried out at 125 °C for 5 h. After the hydrogenation reaction, the obtained polymer was precipitated immediately from ethanol. The precipitation was conducted three times repeatedly to purify the obtained hydrogenated polymer. After the purification it was dried at 40 °C for 24 h under vacuum. s-hPNB was obtained quantitatively; meso/racemo = 10/90 and cis/trans = 100/0.

Isotactic poly(norbornene) (*i*-PNB): Toluene solution of MoO(racemic-5,5',6,6'-tertamethyl-3,3'-ditert-butyl-1,1'-biphenolate)₂ (0.0515 g, 56.7 μmol) was mixed with two equivalents of n-BuLi at 78 °C, and the mixture (deep-blue solution) was allowed to warm to ambient temperature. The mixture was aged for an additional 15 min resulting in becoming a reddish-orange solution. A cyclohexane solution

of NB (7.50 g, 79.7 mmol) and 1-octene (0.225 g, 1.99 mmol) was added to the catalyst mixture at 80 °C. After stirring for 3 hours, the polymerization was quenched with a small amount of ethanol. The obtained polymer was precipitated from ethanol and dried at 40 °C for 24 h under vacuum. *i*-PNB was obtained quantitatively: $M_n = 34,000$ g/mol, $M_w/M_n = 5.2$.²⁹

Isotactic hydrogenated poly(norbornene) (i-hPNB): p-xylene solution of i-PNB and a p-xylene solution of 4 equiv. of p-Tos-NHNH₂ were mixed in a glass flask equipped with a three-way stopcock. The mixture was allowed to heat up to the reaction temperature while stirring. Chemical transfer hydrogenation was carried out at 125 °C for 5 h. After the hydrogenation reaction, the obtained polymer was precipitated immediately from ethanol. The precipitation was conducted three times repeatedly to purify the obtained hydrogenated polymer. After purification, it was dried at 40 °C for 24 h under vacuum. i-hPNB was obtained quantitatively: meso/racemo = 100/0 and cis/trans = 100/0. General Remarks. Norbornene (Tokyo Kasei) was distilled from MS-3A and stored as a cyclohexane solution. 1-Octene (Wako Chemicals) was distilled over calcium hydride. Phenyl isocyanate (Tokyo Kasei) was distilled from calcium hydride. (1,3-bis(2,4,6-trimethylphenyl)-2-imidazolidinylidene) dichloro(benzylidene)(tricyclohexylphosphine)ruthenium (Aldrich), Et₂Al(OEt) (Kanto Chemical), n-BuLi (Kanto Chemical), p-Tos-NHNH2 (Aldrich), WCl6 (Soegawa Chemical), MoOCl4 (Strem) and racemic-5,5',6,6'-tertamethyl-3,3'-di-tert-butyl-1,1'-biphenyl-2,2'-diol (Strem) were used without further purification. Hexamethyldisiloxane (Aldrich) was distilled over molecular sieves under reduced pressure. W(=NPh)Cl₄·Et₂O was synthesized from WOCl₄ and phenyl isocyanate as previously reported.³⁰ MoO(racemic-5,5',6,6'-Me4-3,3'-t-Bu2-biphenolate)₂ (MoO(rac-Biphenolate)₂) prepared from MoOCl₄ and phenolates in diethyl ether as previously reported.³¹

2.2. GPC and Solution-state NMR. The molecular weight distributions (*D*) of the polymers were measured on a gel-permeation chromatograph (GPC) (Tosoh HLC-8320 GPC; eluent tetrahydrofuran).

The relative number- and weight-average molecular weights (M_n and M_w , respectively) were acquired via a calibration curve obtained using polystyrene standards. ¹H and ¹³C solution-state NMR spectra were recorded on a Bruker Avance III 500MHz spectrometer (500.13 MHz for ¹H, 125.77 MHz for ¹³C) with CryoprobeTM DCH 500/3 at 60 °C or on a Bruker Advanced III HD 600 MHz spectrometer (150.91 MHz for ¹³C) equipped with CRYO probe TM DCH 600S3 at 125 °C. Chemical shifts were determined with reference to the tetramethylsilane (0.00 ppm), tetrachloroethane (5.97 ppm for ¹H, 73.8 ppm for ¹³C) or chloroform (7.24 ppm for ¹H, 77.2 ppm for ¹³C). Meso/racemo ratios were determined by peak fitting of ¹³C NMR spectra using Lorentzian function on JEOL Delta v5.0.2 NMR software. Glass transition temperature (T_g) for s-, i-, and a-hPNB was determined to be 5, 5, and 4 °C, respectively, by DSC. For the NMR experiments, the a- and s-hPNB samples were prepared by heating the fresh powders by 10 °C/min in hot stage up to 20 °C above melting temperature and holding for 15 min to eliminate thermal history and cooled down with a rate of 10°C min⁻¹ to ambient temperature. To avoid crystal-crystal transition, fresh i-hPNB powder was used after annealing at 100 °C for 12 hours under vacuum. For SAXS measurement, the melt-crystallized samples were prepared by isothermal crystallization in DSC chamber. The initial temperatures were set at 160, 160, and 200 °C for a-, s-, and i-hPNB samples respectively to make the samples in a molten state. The samples were then cooled down to various crystallization temperatures with a cooling rate of 150 °C min⁻¹ and kept for 10–40 minutes before collecting them out of the chamber.

2.3. ssNMR Experiments. The ¹H and ¹³C ssNMR experiments were carried out on a BRUKER AVANCE300 spectrometer, equipped with a 4 mm VT CPMAS NMR probe. The ¹H and ¹³C carrier frequencies are 300.1 and 75.6 MHz, respectively. The ¹H broad line NMR spectra were obtained by solid echo sequence of ¹H 90° pulse length of 2.2 μs and a delay time of 7 μs. Recycle delay and accumulation number were 4 s and 64, respectively. One ¹H NMR experiment took about 4 min with an

interval of 5 min between two experiments. In the ¹³C MAS NMR experiment, the MAS frequency was set to 4000 ± 3 Hz. The 90° pulses for ¹H and ¹³C were adjusted to 3.3 and 4.5 µs, respectively. The recycle delay and ramp cross-polarization (CP) time were 2 s and 1ms, respectively. High-power ¹H TPPM decoupling with a field strength, $\gamma B_1/2\pi$, of 75.8 kHz was used during ¹³C acquisition time. The chemical shift was referenced to the CH signal of adamantane (29.5 ppm). ¹³C spin-lattice relaxation time in the laboratory frame (T_{1C}) was measured by using Torchia sequence with 13 C 90° pulse length of 4.5 μ s. The ¹H spin-lattice relaxation time in the rotating frame (T_{10H}) measurement was conducted under a spin-locking field strength of 62.5 kHz. ¹H-¹³C WISE spectra were obtained by inserting dwell time of 7 µs with 128 points along t_1 dimension. A short CP time of 100 µs was used to suppress spin diffusion effect. ¹³C CSA was measured by using separation of undistorted powder patterns by effortless recoupling (SUPER).³² ¹H spin-locking filter (T_{10H}) with a filed strength of 62.5 KHz and a pulse duration of 5-20ms was used to suppress the amorphous component. These experiments were performed at MAS frequencies of 3 kHz. The scaling factor, χ', was 0.155. Effective spectral width in the indirect dimension was 3 kHz / 0.155 = 19 kHz. The angular frequency of rf field strength of 13 C 2π pulse, ω_c was set to $12.12\omega_r$. ¹H continuous wave (CW) decoupling with a field strength of 100 kHz was applied during CSA recoupling. The number of t_1 increments was set to 80 in states-TPPI mode. The Center-band Only Detection of Exchange (CODEX)33 experiments utilize the recoupling of CSA interaction by 180° pulses trains in the two evolution periods sandwiching a mixing period, t_{mix} . The effect is a signal decay due to the dephasing of magnetization brought about by changes in orientationdependent CSA due to reorientation dynamic process during t_{mix} . The magnetization evolves during the initial evolution period $Nt_r/2$ (where N=2, 4, 6, ...) under the orientation-dependent CSA interaction, which is recoupled by two successive 180° pulses per MAS rotation period, t_r . The magnetization after the first evolution period is stored along the z direction by a 90° pulse and does not dephase during $t_{\rm mix}$ (which must be set to an integer multiple of t_r). The magnetization evolves again after the 90° readout

pulse during the second evolution period $(Nt_r/2)$ and is refocused at its end. The second mixing period t_z serves as a z-filter and permits the cancellation of longitudinal relaxation. t_z was set to one t_r . After applying the last 90° pulse, the signal was detected under ¹H TPPM decoupling. The resulting dephasing leads to a decay of the signal-intensity in the exchange spectrum (S). To remove the T_1 and spin-spin relaxation (T_2) effects during t_{mix} and Nt_{r} , a reference spectrum is acquired. It is obtained simply by interchanging t_{mix} and t_z . The signal intensity in the reference spectrum (S_0) is not sensitive to exchange processes but is only dominated by T_1 , T_2 , and pulse length errors. The motional correlation time and information about the motional geometry can be obtained by plotting the ratio (S/S_0) versus t_{mix} and (S/S_0) versus Ntr, respectively. In a longer $t_{\text{mix}} > 1.0$ s, spin diffusion contributes to S/S_0 . Spin diffusion correction was conducted by $(S/S_0)^* = (S/S_0)/(S/S_0)_{SD}^{34}$ where $(S/S_0)_{SD}$ was obtained at -5 °C. The MAS frequency was 4000 ± 3 Hz. The ¹H rf field strength for CW decoupling during ¹³C 180° pulse with pulse length of 15 μ s was set to 76 kHz. A short CP time of 100 μ s or $T_{1\rho H}$ filter with spin-locking field strength of 62.5 kHz was used to suppress the amorphous signals to the CODEX experiments at varied temperatures. All other rf parameters were the same as for the CPMAS experiments. The reference and exchange experiments were obtained alternatively by every 128 transients, to suppress drift of the NMR spectrometer. Each spectrum was obtained by accumulating 1024–2048 transients.

- **2.4. DSC.** DSC experiment was conducted using TA Discovery DSC250 with heating and cooling rates of 10 °C/min in N₂ atmosphere. Temperature and heat flow were calibrated by standard sample.
- **2.5. SAXS.** SAXS measurements were performed at the beamline 19B2 in SPring-8 (Hyogo, Japan). The energy of the incident X-ray beam was 18 keV. The scattered X-ray was detected by Pilatus 2M. The sample-to-detector distances were 3 m for normal SAXS and 42 m for U-SAXS. The obtained 2D images were converted into 1D profiles and corrected with transmittance, irradiation time and background.

3. RESULTS

3.1. Thermal Properties of hPNBs. Fig. 1a-c depicts DSC thermograph of a-, i-, and s-PNBs. During the heating process a- and i-hPNBs experience crystal-crystal transition at T_{cc} of 115 and 150 °C, while s-hPNB does not. The T_{m} for s-, i-, and a-hPNBs are 135, 178, and 145 °C, respectively. Crystallization temperature (T_{c}) for s-, i-, and a-hPNBs are 113, 138, and 123 °C. It is important to note the temperature difference between T_{m} and T_{c} , (T_{m} - T_{c}) for three samples. T_{m} - T_{c} for a- and s-hPNBs are 22 °C while i-hPNB is 40 °C. This physical property will be discussed in detail in section 4.1.

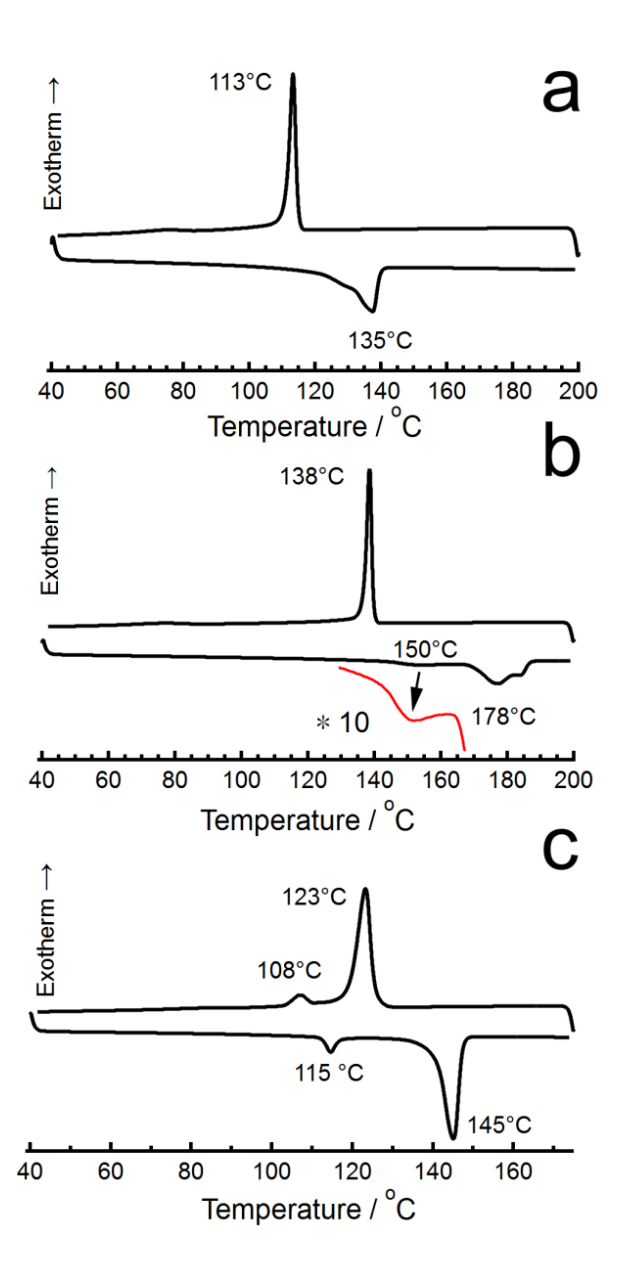


Figure 1. DSC thermograph of (a) s-, (b) i-, and (c) a-PNBs with heating and cooling rates of 10 °C/min.

3.2. ¹H broad-line NMR and Crystallinity. Fig. 2a-c displays ¹H broad-line NMR spectra for *a*-hPNB at 25 °C, 105 °C, and 117 °C. At 25 °C, only one broad component with full width at half maximum (FWHM) of ca. 40 kHz was observed. With increasing temperature, segmental motions of the amorphous components are thermally activated ($T_g \sim 3$ °C), which leads to narrowed ¹H signals well above T_g . Above 80 °C, two components are clearly observed in Fig. 2b, c. Lorentzian and Gaussian peaks were applied to the observed NMR line-shapes above 80 °C. The ¹H broad-line NMR spectra for s-, i-, and a-PNBs obtained at 90 °C are shown in Fig. 2d-f. The Φ_c of s-, i-, and a-hPNBs was determined to be 50%, 48%, and 80% at 90 °C. Fig. 2g-i illustrates Φ_c of s-, i-, and a-hPNBs, respectively, during heating (blue filled circle) and cooling (green) processes determined by ¹H line-shape analysis.

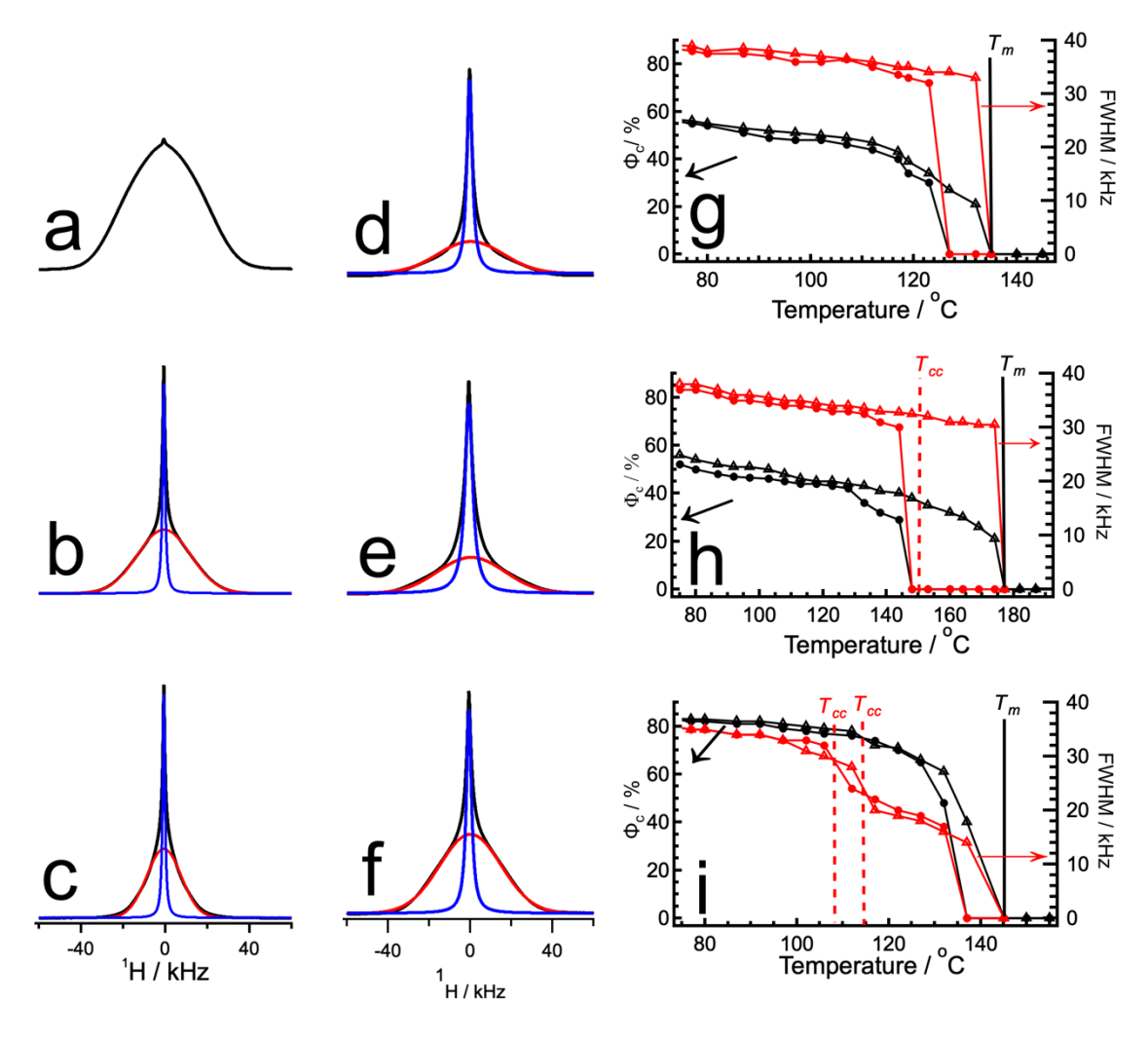


Figure 2. ¹H broad-line NMR spectra for *a*-hPNBs at (a) 25, (b) 105, and (c) 117 ° C. ¹H broad line NMR spectra for (d) *s*-, (e) *i*- and (f) *a*-hPNB at 90 °C. Gaussian and Lorentzian peaks being fitted to the experimental curves above 80°C. Crystallinity (black circles and triangles) and ¹H FWHM (red circles and triangles) for the crystalline regions of (g) *s*-, (h) *i*- and (i) *a*-hPNB during heating (triangles) and cooling processes (circles). ¹H NMR experiment time of about 4 min with an interval of 5 min between the experiments.

The cooling process from the melt induces crystallization of i- and s-hPNBs at around 145 °C and 125 °C respectively. The observed T_c for i- and s-hPNBs in the 1 H NMR experiments are higher by 8 °C and 12 °C, respectively when compared to those seen by DSC. The higher T_c values are accounted for from slow kinetics used in the 1 H NMR experiments. Φ_c of i- and s-hPNBs reaches 50% and 55%, respectively at 80 °C. For a-hPNB, onset temperature for crystallization is at around 136 °C in the NMR experiment. The crystallinity rapidly increases up to 75% at 120 °C above T_{cc} and reaches a maximum value of 82% at 80 °C. The determined crystallinity of a-hPNB is well consistent with the reported value (78%) by Register and coworkers. 26

Fig. 2g-i plots FWHM of the crystalline component of s-, i-, and a-hPNBs, respectively, during heating (red filled triangle) and cooling process (black). In the cooling experiment, i- and s-hPNBs, show FWHMs of 30 kHz at 145 °C and 32 kHz at 124 °C, respectively. These line widths do not vary during cooling and heating processes. On the other hand, when a-hPNB crystallizes during cooling, the crystalline component with FWHM of 18 kHz appears at 132 °C. The line-width gradually increases to 24 kHz at 115 °C but drastically increases up to 35 kHz at 105 °C below T_{cc} . Also, similar discrete transition in FWHM was observed at around T_{cc} during heating process (**Fig. 2b, c, and i**). These behaviors indicate that only a-hPNB undergoes significant molecular dynamics in the frequency range

of over ~40 kHz above T_{cc} . Note that similar reduction of 1 H linewidth was observed in PE above a critical pressure and temperature 9 and in iPB1 form II. 35

3.3. 13 C High-Resolution NMR and Crystallinity. Fig. 3a-c represents 13 C CPMAS NMR spectra (black lines) for s-, i-, and a-hPNBs measured at 25 °C and signal assignments. ^{26, 29} Fig. 3d shows 1 H spin-lattice relaxation time in the rotating frame $(T_{1\text{pH}})$ curves for s- (black filled circles), i- (red), and ahPNBs (blue) at 25 °C. The relaxation curves for all three samples were analyzed in terms of double exponential curves. Fig. 3d describes the best fit curves with the parameters for relaxation values of crystalline (T_{10HC}), amorphous components (T_{10HA}). The relative fraction of the amorphous components (f_a) is listed in **Table 2**. The T_g for all three samples are ~ 3 °C. The short and long relaxation values are assigned to the amorphous and crystalline components. With a spin locking time of 20 ms, the majority of the amorphous components ($T_{1\rho HA} = 4.7-6.3$ ms) decay and thus the crystalline components dominate the spectra (red dotted ones in Fig. 3a-c). The 1 H magnetization of the crystalline components for s-, i-, and a-hPNBs, M ($t_{\rm sl} = 20$ ms) decays to 0.78 (decaying factor), 0.57, and 0.50* M_0 respectively, where M_0 is an initial size of the magnetization at $t_{\rm sl} = 0$ ms. The full crystalline signals for s-, i-, and a-hPNBs can be obtained by $M(t_{\rm sl}=20~{\rm ms})/{\rm decaying}$ factor and were depicted as red solid curves in Fig. 3a-c. Subtraction of the full crystalline signals from the CPMAS spectra produces the amorphous component illustrated as blue solid spectra depicted in Fig. 3a-c. All three samples show similar spectra for the amorphous components. The remaining crystalline signals highlighted by red show very similar chemical shift values for all the functional groups across three samples. This result suggests that s- and i-hPNBs adopt similar trans-conformation in the crystalline region to that in a-hPNB. The detailed conformation and packing structure are under investigation by X-ray diffraction analysis. ¹³C CPMAS NMR spectra for all three samples at elevated temperatures are displayed in Fig. S1-3. With increasing temperature, the broadened amorphous signals are narrowed due to thermally activated molecular

dynamics. Therefore, the crystalline signals for C2,3 and C1,4 carbons are well separated from the corresponding amorphous signals at high temperatures.

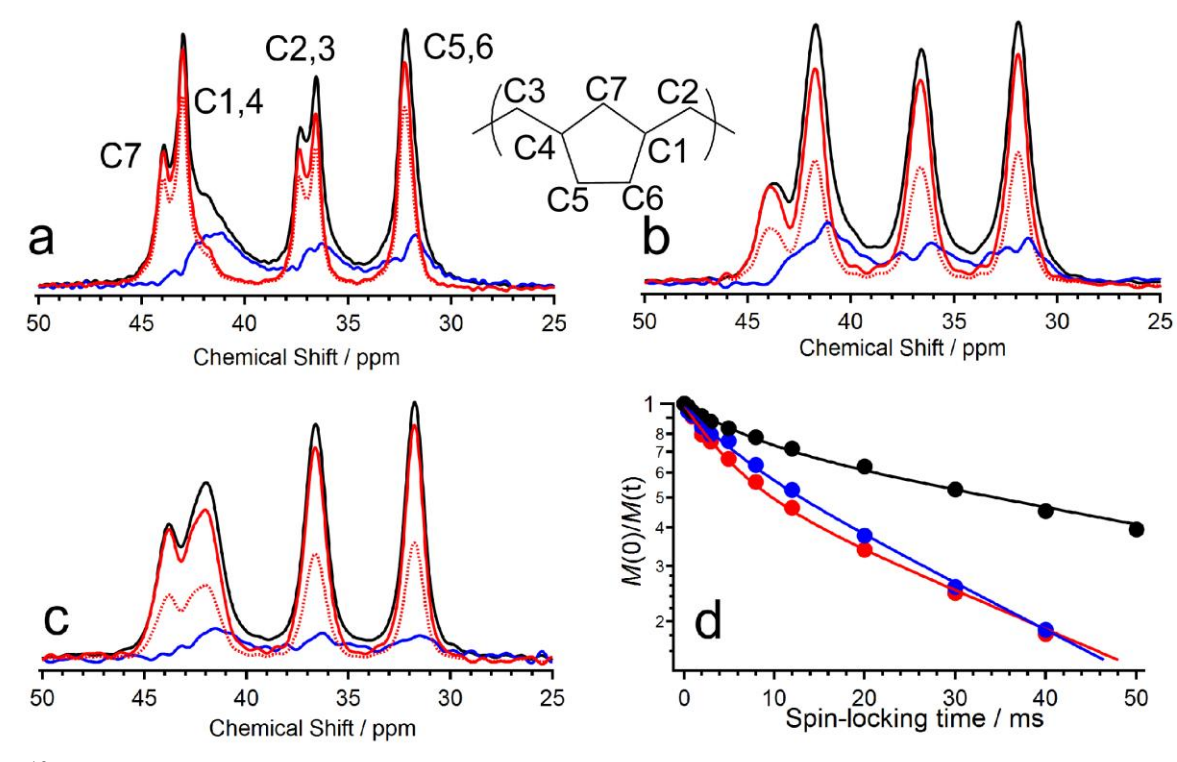


Figure 3. ¹³C CPMAS NMR spectra (black) and $T_{1\rho H}$ filtered CPMAS spectra (dashed red) for (a) s-, (b) i-, and (c) a-hPNBs at 25 °C. (d) $T_{1\rho H}$ relaxation curves for s- (black filled circle), i-(red), and a-hPNBs (blue). The crystalline spectra being obtained by $T_{1\rho H}$ filtered CPMAS spectra with a duration of 20 ms divided by exp(-20/ $T_{1\rho HC}$). (a-c) The amorphous spectrum (blue) being obtained by subtraction of the crystalline spectrum (red) from the CPMAS one (black).

Table 2. $T_{1\rho H}$ values for the crystalline and amorphous regions for s-, i-, and a-hNBs obtained through C1,4 carbons at 25°C

	$T_{1 m ho HA}/ m ms$	$T_{ m 1 ho HC}$ /ms	$f_{ m a}$
s-hPNB	6.3 ± 0.9	80.0 ± 5.8	0.25 ± 0.01
i-hPNB	4.7 ± 0.4	35.0 ± 3.2	0.41 ± 0.05
a-hPNB	5.2 ± 0.6	29.0 ± 4.5	0.25 ± 0.01

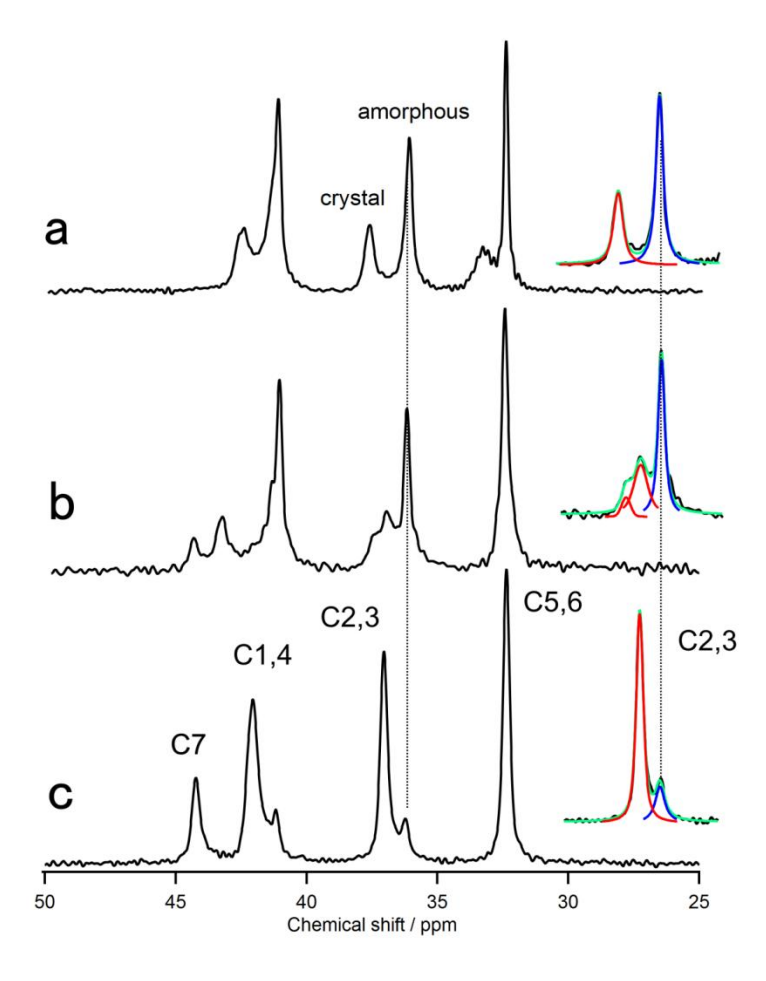


Figure 4. ¹³C DPMAS NMR spectra for (a) i-hPNB at 155 °C, (b) s-hPNB, and (c) a-hPNB at 117 °C. Recycle delay was set to 5x the longest ¹³C T_1 values in the systems (i-hPNB, 35 s, s-hPNB, 1500 s and a-hPNB, 10 s). The crystallinity of i- (40%), and s- (45%) and a-hPNB (80%) is determined by applying Lorentzian peaks to the crystalline (red) and amorphous (blue) peaks for the C2, 3 carbons.

 13 C direct polarization magic-angle spinning (DPMAS) NMR spectra for the s-, i-, and a-hPNBs under high-power 1 H decoupling were measured at 117 $^{\circ}$ C, 155 $^{\circ}$ C, and 117 $^{\circ}$ C and were shown in **Fig.** 4, where the recycle delay was set to a time >5x the longest 13 C spin-lattice relaxation time in the laboratory frame (T_{1C}) (see **Table S1**). The longest T_{1c} values are 291 s, 7.2 s, and 1.6 s for s-, i-, and a-hPNBs crystalline regions, respectively. The large variations in the T_{1C} values indicate that chain dynamics are largely different in the crystalline region among three samples. Detailed molecular

dynamics will be discussed in the later section. Among four carbon signals, C1,4 and C2,3 cabons show the crystalline and amorphous signals separately. The C2,3 signals appear to have better peak separations between them. Thus, the C2,3 signals were utilized to determine crystallinity for *s*-, *i*-, and *a*-hPNBs to be 42%, 40%, and 80%, respectively. These results are consistent with ¹H NMR results depicted in **Fig. 2g-i**. The unique trend in crystallinity of hPNBs can be compared with existing literatures. Among various polymers, poly(vinyl alcohol) (PVA), for poly(acrylonitrile) (PAN), and poly(vinyl chloride) (PVC), crystallize in *atactic*-configurations. The reported crystallinities of *a*-PVA, for a-PAN, a-PVC, are 30%, < 50%, and 10%, respectively. All the reported values of crystallinity in several *atactic*-polymers are much lower than that of *a*-hPNB.

3.4. Long period by SAXS and USAXS. Fig. 5a-c demonstrates the L of s-, i-, and a-hPNBs at various crystallization temperature (T_c), investigated by small and ultra-small angle X-ray scattering (SAXS and USAXS). s-hPNB exhibits its T_c independent of q_{max} of 0.30–0.31 nm⁻¹. The q_{max} value corresponds to L = 20-21 nm in terms of $L = 2\pi/q_{\text{max}}$. i-hPNB shows similar values of 17–21nm. Interestingly, L of 17 nm was obtained at the highest T_c of 135 °C. This is opposite trend in temperature dependence of L and lamellae thickness of semicrystalline polymers. This unique temperature dependence of L will be discussed in a later section. Scattering pattern for a-hPNB shows first- and second-order peaks. The latter highlighted by asterisks arises from structural homogeneity. The large L values were determined by the first-order peak and highly depend on T_c : the L value corresponds to 49 nm at $T_c = 95$ °C and increases to 55 nm at 105 °C, 68 nm at 115 °C, and 80 nm at 125 °C as shown in Fig. 5c. The observed T_c dependence of L for a-hPNB is well consistent with the previous result. ²⁸ The L value for a-hPNB is four times greater than those of s- and i-hPNBs. Both crystallinity and L clearly show unique structural developments of a-hPNB compared to stereo-regular ones. To the best of our knowledge, this is the first report of an *atactic*-polymer exhibiting a much higher crystallinity and much longer L of than its stereo-regular counterparts.

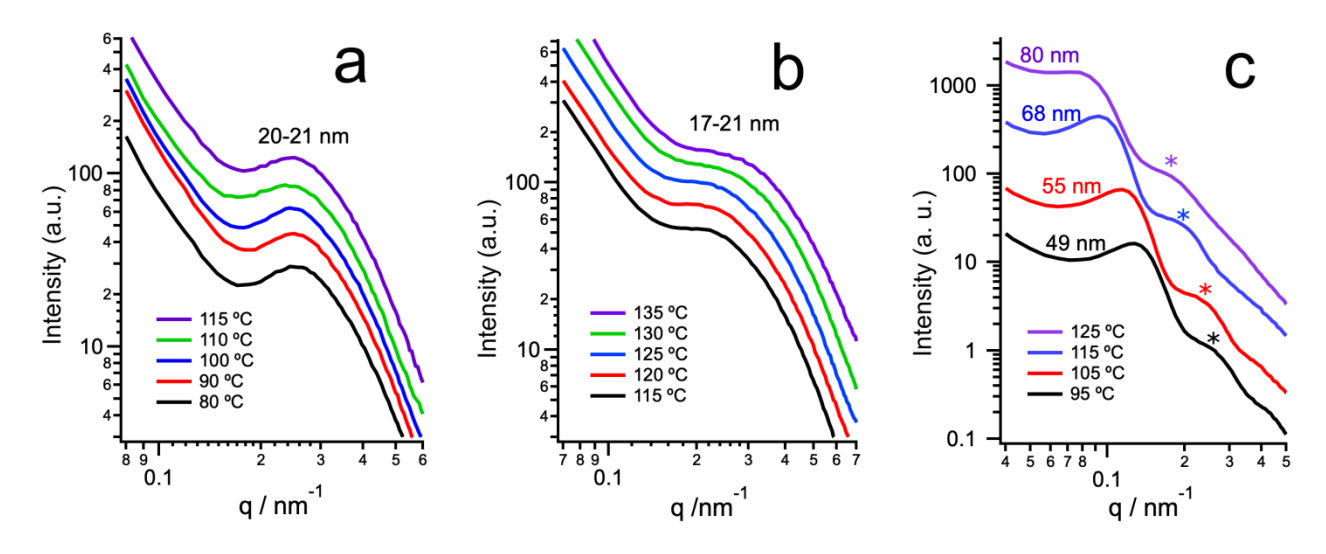


Figure 5. SAXS and USAXS data for (a) *s*-hPNB, (b) *i*-hPNB, and (c) *a*-hPNB crystallized at various temperatures. * representing second-order peak.

3.5. Slow Dynamics of Crystalline Regions of hPNBs below T_{cc} . CODEX provides detailed molecular dynamics including amplitude and kinetics of molecular motions in the slow dynamic regime $(10^{-2}-10^2 \text{ s})^{.33}$ Fig. 6a-c shows CODEX³¹ reference (S_0) and exchange $(S)^{13}$ C NMR spectra for s-, i- and a-hPNB, respectively, with a mixing time (t_{mix}) of 200 ms and evolution time (t_{evo}) of 4.5 ms. The amorphous peaks were suppressed by using a short CP time of 100 μ s. For s-hPNB, intensities of all the peaks in S are very similar with those in S_0 (S/S_0 intensity ratio ~ 1.0). On the other hand, a-hPNB shows S/S_0 ratios of 0.84 (C1,4) - 0.48 (C5,6) within t_{mix} of 200 ms at 110 °C (Fig. 6c). Similarly, i-hPNB gives the S/S_0 ratios of 0.65 - 0.87 at 135 °C below T_{cc} (Fig. 6b).

Fig. 6d depicts temperature dependence of the S/S_0 ratio for the C5,6 carbons for s-, i-, and a-hPNBs with $t_{\rm mix} = 200$ ms and $t_{\rm evo} = 4.5$ ms. This experiment is referred as 1-point CODEX. For s-hPNB, the S/S_0 ratio is almost invariant (~1) up to 125°C just below $T_{\rm m}$. This means that s-hPNB chains do not conduct any reorientation of the CSA tensors within 200 ms up to $T_{\rm m}$. On the other hand, the S/S_0 ratio for a- and i-hPNB exhibits temperature dependence: In the former, the S/S_0 ratio continuously decreases with increasing temperature up to 110 °C just below $T_{\rm cc}$, and the S/S_0 ratio jump up to ~ 1 at 122 °C,

slightly above T_{cc} . This implies that a sudden change in the motional frequency occurs across T_{cc} . In the latter, the S/S_0 ratio starts to decrease above 60 °C and reach 0.67 at 108 °C. Even with further increasing temperature, the ratio of ca. 0.65 is almost invariant up to 140 °C. This result implies that the slow dynamics are not thermally activated in i-hPNB due to unknown structural factors within the temperature range above 108 °C. We will further investigate this unusual dynamic behavior of i-hPNB. At 160 °C above T_{cc} , the ratio quickly increases to \sim 1. This observation is the same in the CODEX result for a-hPNB. To understand dynamic sources for $S/S_0 = 1$ above T_{cc} , we will further study molecular dynamics of both a- and i-hPNBs above T_{cc} in section of 3.8.

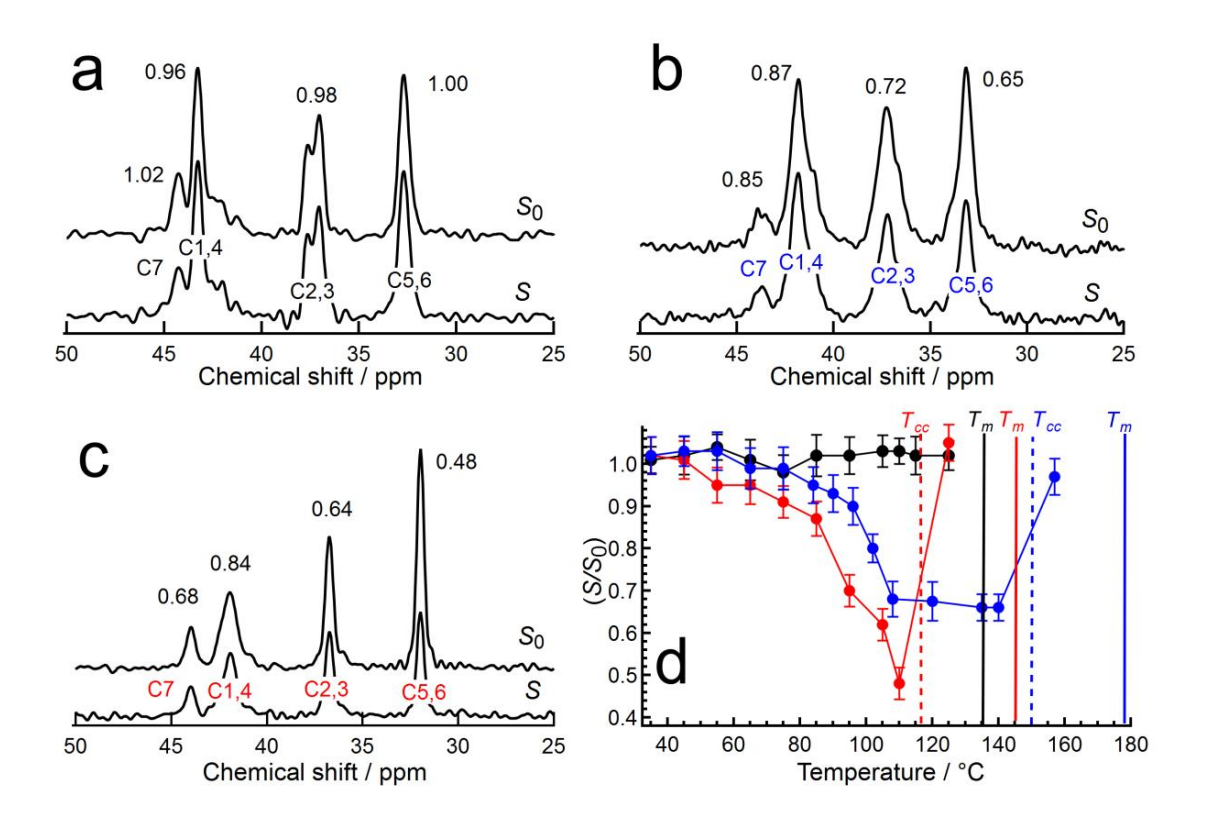


Figure 6. CODEX reference (S_0) and exchange (S_0) and exchange (S_0) and exchange (S_0) in the spectra for (a) S_0 , (b) S_0 in and (c) S_0 and (c) S_0 with a mixing time (S_0) of 200 ms and evolution time (S_0) of 4.5 ms at 110 °C, 135 °C, and 110 °C, respectively. (d) Temperature dependent CODEX (S_0) ratio of C5,6 carbons in S_0 (blue), S_0 in the second of the spectra for (a) S_0 in and S_0 in the spectra for (a) S_0 in the spectra for (b) S_0 in the spectra for (

To investigate the reorientation angle for the atomic dynamics, principal axis values of chemical shift anisotropy (CSA) are necessary. CSA patterns for a- hPNB were measured by SUPER³² combined with a $T_{1\rho H}$ filter at 25 °C. Fig. 7a shows CSA patterns for a-hPNB crystalline region at 25 °C. The principal values are listed in **Table S2**. **Fig. 7b**. depicts CODEX t_{evo} dependence of the S/S_0 ratio for all carbons of a-hPNB with a mixing time of 200 ms at 110 °C. It was found that the decaying degrees highly depend on the atomic sites (C5,6 >, C2,3 \approx C7,> C1,4) and do not reach minima at t_{evo} of 4.5 ms. Here, we conduct molecular dynamics analysis of the C7 carbon for a-hPNB where it was assumed that CSA tensor adopts the same orientation with the methylene carbon of PE.³² We supposed two dynamic models: One is rigid body model where the chain conducts rotations around its chain axis, the second where cooperative C-C internal bond rotations apparently induce re-orientations of CSA tensors at each carbon site.). Two kinds of motions of 180° flip with reorientation angle, $\theta = 180^{\circ}$ and uniaxial diffusions with $\theta = 0-360^{\circ}$ are considered. The simulation curve for the 180° flip shows no decay as a function of evolution time due to invariant CSA orientations before and after the flip and is consistent with the simulation with reorientation angle of 0°. To calculate uniaxial diffusion around its chain axis, reorientation angles of $\theta = 0-90^{\circ}$ with every 5° intervals were calculated and summed up with an equal probability. The simulation curves for 90° flips and uniaxial rotations were represented as solid curves in Fig. 7f. None of three calculated curves fit to the experimental data. Namely, neither diffusion type of motions with reorientation angles of 0-360° nor discrete jumps with reorientation angles of 90 and 180° occur in a-hPNB crystalline region. These comparisons clearly indicate that the observed slow dynamics in a-hPNB are different from the previously reported dynamics in mobile crystals such as PE, ³⁷ poly (ethylene oxide) (PEO), ³⁸ poly(oxymethylene) (POM), ³⁹ isotactic-poly(propylene) (i-PP), ^{12,13} isotactic-poly(4-methyl-1-penetene) (i-P4M1P), 40 poly (L-lactic acid) (PLLA), 41 isotactic-poly(1butene) (i-PB1) form III⁴² which commonly conduct large amplitude motions with reorientation angles of 75–200°. The second model considered utilizes cooperative rotations around individual C-C internal bonds in hPNB lead to reorientation of CSA tensors with a limited angle at each carbon site. It is known that cyclopentane adopts puckered conformations and conducts conformational transition as well as rotations in the solid crystalline phase above -172 °C.²² This suggests that conformational change in cyclopentyl group could occur in both a-and i-hPNBs (**Fig. 7e**). An assumption in this approach is that a vector from center of mass of cyclopentyl ring to each carbon is changed due to individual C-C bond rotations as schematically illustrated in **Fig. 7d**. Such dynamics may show a relatively small reorientation angle, θ compared to the rigid body dynamics around its chain axis.

Fig. 7g shows CODEX t_{evo} dependence of S/S_0 for the C7 carbon of a-hPNB and simulation curves under the assumptions of two-sites with the reorientation angle, $\theta = 5$ -30° (black curve). None of the simulated curves fit the experimental curve. The simulation curve with $\theta = 20^\circ$ is the closest to the experimental data, however it deviates from the experimental data in the late stage of t_{evo} . Under the assumption of a box-type of distribution including reorientation angle of 5-30° with 1° step, the weight-averaged simulation curve (red curve) could reproduce the experimental data with improved accuracy. The distribution of the small amplitude motions means that two-site jump occurs not in discrete energy minima but in rather flat ones. This means that the cyclopentyl ring is not limited to two conformations but is flexible and adopts multiple conformations. The characteristic reorientation angles of 5-30° in a-hPNB are quite unique compared to other mobile crystals such as PE, 37 i-PP, 12,13 PEO, 38 i-P4M1P, 40 i-PB1 form III, 42 PLLA, 41 etc. which achieve high reorientation angles (75-200°) depending on their conformations. Register and coworker investigated crystal unit-cell parameters of a-hPNB below T_{cc} and reported the 0.5% contraction of the c-axis dimension between 23 and 95 °C. 26 The contraction is well consistent with the presence of small amplitude motions in the a-hPNB crystalline region.

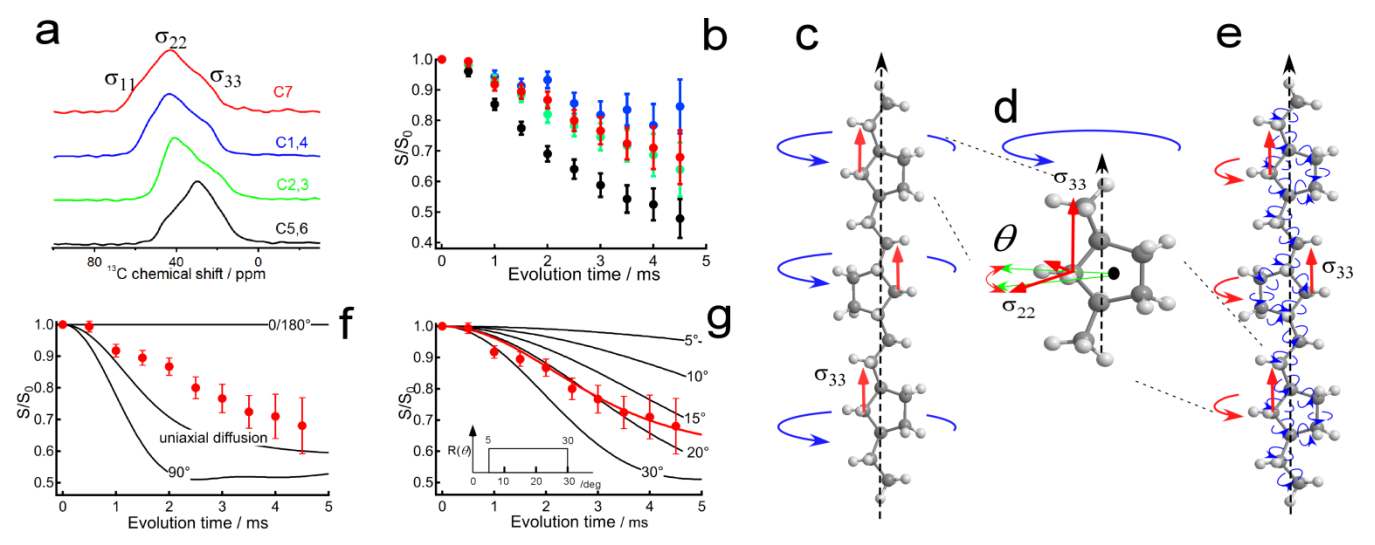


Figure 7. (a) ¹³C CSA spectra for *a*-hPNB crystalline region at 25 ° C. (b) CODEX t_{evo} dependence of S/S_0 for C5,6 (black filled circle), C1,4 (blue), C2,3 (green), and C7 (red) of *a*-hPNB with t_{mix} of 200 ms at 110 °C. Schematic illustration for molecular dynamics for *a*-hPNB in (c) rigid body and (e) C-C internal bond, and (d) expanded cyclopentyl group and reorientation angle (θ) effect on CSA orientations on the C7 carbon. CODEX t_{evo} dependence of S/S_0 for C7 and simulation results (solid black line) based on (f) 90°, 180° flips and uniaxial diffusion around the chain axis and (g) two-site jumps with a small reorientation angle, $\theta = 5-30^{\circ}$ (black solid line) and two-sites jumps with box-type distribution of $\theta = 5-30^{\circ}$ (red curve).

Fig. 8a, b shows CODEX t_{mix} dependence of $(S/S_0)^*$ for the C5,6 carbons for a- and i-hPNB with a fixed t_{evo} of 3ms. Since spin exchange is a result of both molecular dynamics and spin diffusion occurs at a mixing time on the order of seconds, steps must be taken to eliminate the latter process. ³⁴ In order to eliminate spin-diffusion effect on the CODEX S/S_0 curves, pure spin-diffusion effect, $(S/S_0)_{SD}$ was measured at -5 °C below T_g and spin-diffusion correction was conducted in terms of $(S/S_0)^* = (S/S_0)/(S/S_0)_{SD}$ (see Figure S4). ³⁴ For a-hPNB, the CODEX decaying curves get deeper and deeper with increasing temperature. Similar observations were reported in several mobile polymer crystals such as PEO, ³⁸ i-PP, ^{12, 13} i-P4M1P, ⁴⁰ PLLA, ⁴¹ etc. For i-hPNB, the CODEX t_{mix} decaying curve

for the C5,6 carbon of *i*-hPNB initially follow the similar trend with *a*-hPNB. However, the CODEX curves are almost invariant above 108°C. This unusual result is well consistent with 1-pt CODEX result in **Fig. 4c**.

The CODEX t_{mix} curve was analyzed in terms of:

$$\left(\frac{S}{S_0}\right) * = 1 - a \left(1 - \exp\left(-\frac{\tau_c}{t_{\text{mix}}}\right)^{\beta}\right),$$

where a is related to available site number, p in terms of a = (p-1)/p, β means distribution width of correlation time, τ_c (0 < $\beta \le$ 1).⁴⁰ A smaller β value means a large distribution of τ_c .⁴³ The best-fit parameters were listed in Table 3 and the best-fit lines were drawn as solid lines in Fig. 8a. With lowering temperatures, the CODEX t_{mix} curve for a-hPNB does not show a plateau value. Thus, the analysis was approximated with a fixed a value of 0.54 obtained at the highest temperature of 110 °C. Similarly, the fixed a value of 0.54 was used for the CODEX $t_{\rm mix}$ analysis for i-hPNB (see **Table 4**). $\tau_{\rm c}$ and its distribution width for a- and i-hPNB were plotted as filled circles and error bars in Fig. 8c. Temperature dependence of τ_c for a-hPNB system follows Arrhenius line with an activation energy (E_a) of 191 \pm 16 kJ/mol. Similarly, *i*-hPNB dynamics also follows Arrhenius line with $E_a = 178 \pm 4$ kJ/mol up to 108 °C. Temperature dependence of τ_c starts to deviate from the Arrhenius line above 108 °C. This result is well consistent with the 1-point CODEX results in Fig. 6. To the best of our knowledge, only i-P4M1P shows some bend in temperature dependence of molecular dynamics in the crystalline region. The observed slowing dynamics in the crystalline region was interpreted in terms of association with frozen segmental motions of amorphous segments below $T_{\rm g}$. High temperature bent in molecular dynamics is peculiar for i-hPNB. Configuration differences lead to the different temperature dependence of slow molecular dynamics between i- and a-hPNBs. We will further study molecular dynamics and conformation of a- and i-hPNBs above T_{cc} . The molecular dynamics and structures in the high temperature phase may give hints for unusual molecular dynamics in i-hPNB below $T_{\rm cc}$.

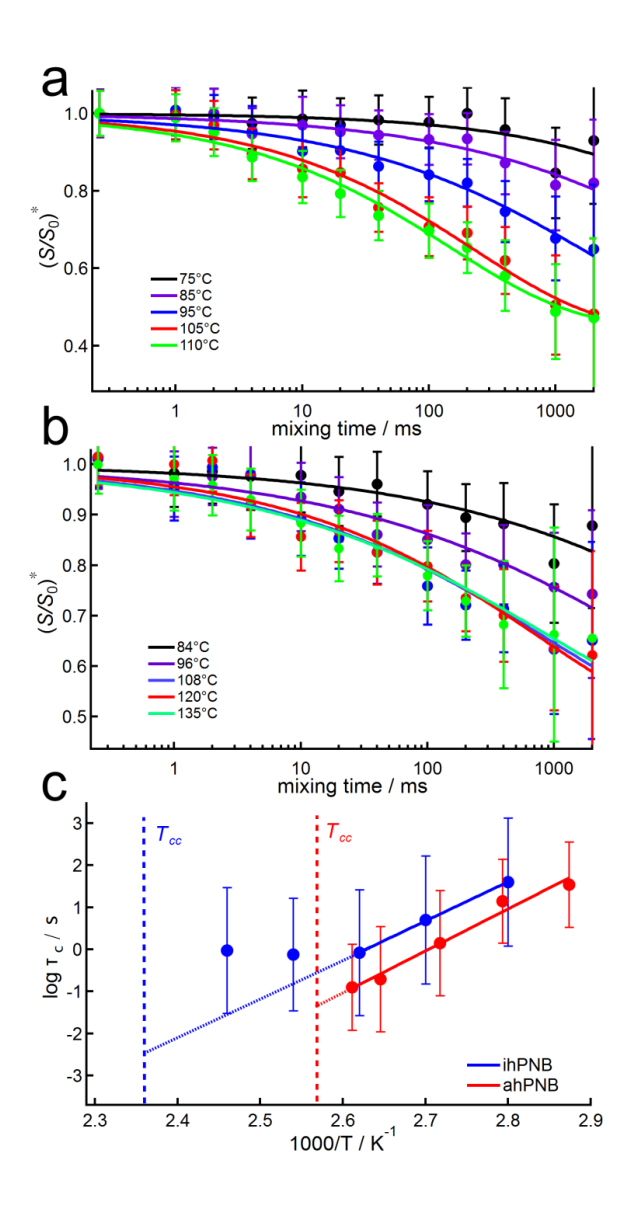


Figure 8. CODEX t_{mix} dependence for $(S/S_0)^*$ of the C5,6 carbons for (a) a- and (b) i-hPNBs with t_{evo} of 4.5 ms at varied temperatures. (c) Arrhenius plots of τ_c for a- and i-hPNBs with best-fit curves of 178 and 194 kJ/mol, respectively.

 $E_{\rm a}$ values for a- and i-hPNBs are much higher than the reported $E_{\rm a}$ values for 180° flips of PE (122 kJ/mol), 37 120° jumps for i-PP (72-102 kJ/mol), 12,13 and ca. 100° jumps for i-P4M1P (95 kJ/mol). Moreover, molecular dynamics of cyclopentyl groups in a- and i-hPNB begins at much higher temperatures than that of cyclopentane. This implies that individual C-C bond rotations are not independent of each other but cooperatively occur with the neighboring groups along the chain axis.

Moreover, parallel packing with neighboring chains also limits the rotation angle. These two structural constraints are possible sources for high energy barriers for the conformational events in a- and i-hPNBs below T_{cc} . s-hPNB does not conduct conformational events as well as crystal-crystal transition. This endorses the idea that conformational events in a- and i-hPNB trigger phase transitions at around 115 and 150 °C, respectively.

Table 3. Best-fitting parameters of the CODEX mixing-time dependence of $(S/S_0)^*$ for C5,6 carbons of *a*-hPNB.

Temperature/ °C	а	$ au_{ m c}/{ m s}$	β
75	$0.54^{1)}$	62.69 ± 6.03	0.45 ± 0.09
85	$0.54^{1)}$	17.86 ± 4.78	0.38 ± 0.04
95	$0.54^{1)}$	1.55 ± 0.29	0.38 ± 0.03
105	$0.54^{1)}$	0.19 ± 0.02	0.46 ± 0.03
110	$0.54^{1)}$	0.12 ± 0.02	0.47 ± 0.04

¹⁾ Fixed a value being used for CODEX analysis.

Table 4. Best-fitting parameters of the CODEX mixing-time dependence of $(S/S_0)^*$ for C5,6 carbons of *i*-hPNB.

Temperature/ °C	а	$ au_{ m c}/{ m s}$	β
84	0.54^{1}	40.13 ± 3.83	0.31 ± 0.06
96	0.54^{1}	5.09 ± 1.87	0.31 ± 0.03
108	0.54^{1}	0.83 ± 0.02	0.33 ± 0.03
120	0.54^{1}	0.75 ± 0.02	0.36 ± 0.04
135	0.54^{1}	0.93 ± 0.03	0.32 ± 0.03

¹⁾ Fixed a value being used for CODEX analysis.

3.8. Molecular Dynamics of hPNBs above T_{cc} . Fig. 9a depicts ¹³C CPMAS NMR spectra for *i*-hPNB below and above T_{cc} . Interestingly, the C7 signal disappears above T_{cc} . The disappearance of the C7 signal above T_{cc} suggests up-field shift, which is due to conformational change to *gauche* one⁴⁴ as schematically drawn in **Fig. 9a**. Currently, detailed XRD analysis is under progress and detailed conformation of *i*-hPNB in the low and high temperature phase will be reported elsewhere.

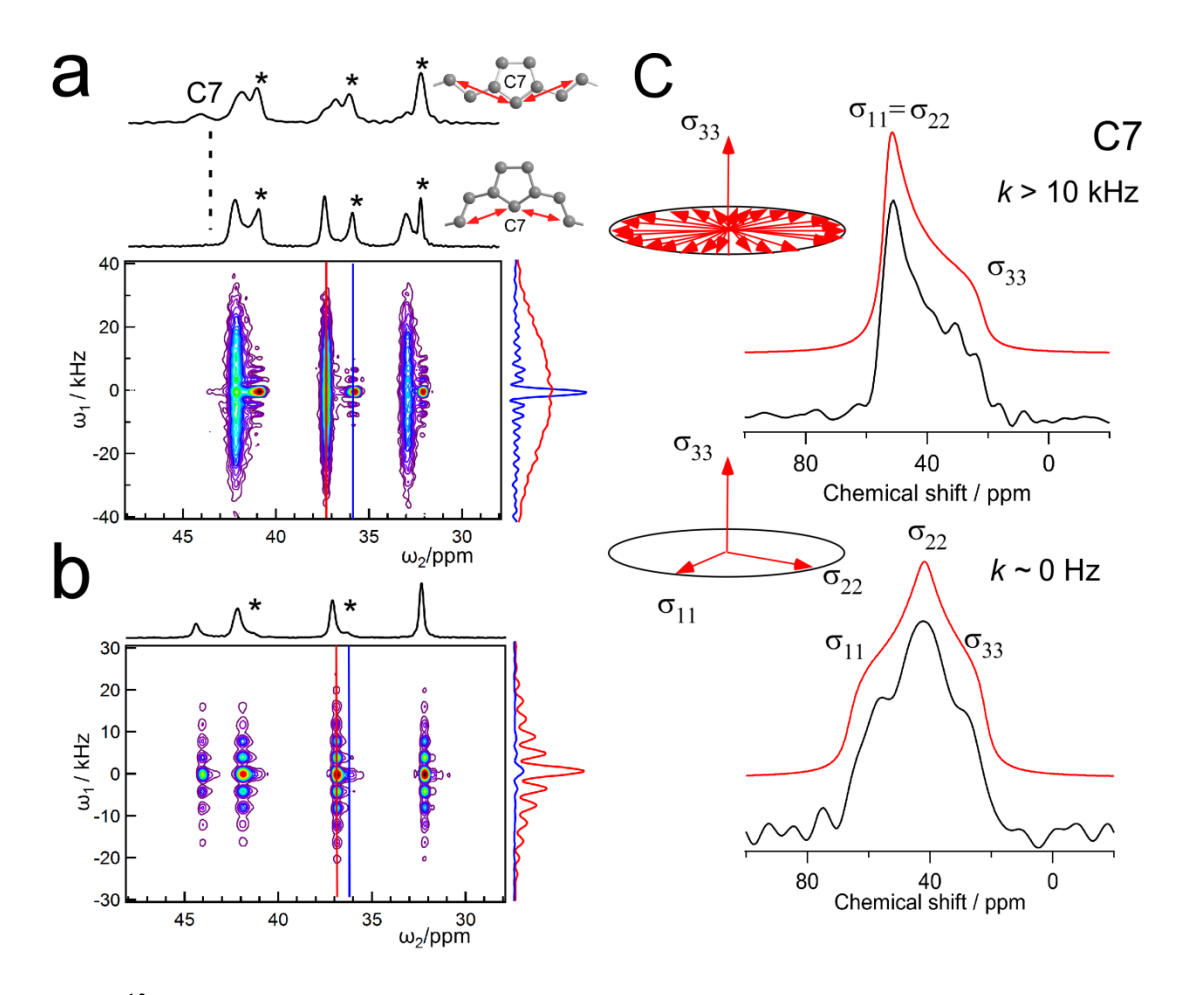


Figure 9. (a) 13 C CPMAS NMR spectra for *i*-hPNB at 145 (top) and 165 $^{\circ}$ C (bottom). Schematic illustration for possible conformation of *i*-hPNB crystalline region below and above T_{cc} . 1 H- 13 C WISE NMR spectra for (a) *i*- and (b) *a*-hPNBs at 165 and 123 $^{\circ}$ C, respectively. * denoting the amorphous signals. The 1 H slice data being shown through 13 C C2,3 signals. (c) 13 C experimental and simulated CSA patterns for C7 of *a*-hPNB crystalline regions at 40 and 123 $^{\circ}$ C.

Fig. 9a shows ${}^{1}\text{H}$ - ${}^{13}\text{C}$ WIdeline SEparation (WISE) spectrum for *i*-hPNB at 165 °C. The ${}^{1}\text{H}$ slice spectra for the ${}^{13}\text{C}$ amorphous signals marked by asterisks clearly illustrate ${}^{1}\text{H}$ isotropic signal accompanying weak ${}^{1}\text{H}$ spinning side band (ssb)s. On the other hand, the crystalline slice indicates ${}^{1}\text{H}$ broadened spectrum with FWHMs of ca. 35 kHz. This means that there is no intermediate and fast molecular dynamics with large amplitudes in the *i*-hPNB crystalline region above T_{cc} . Interestingly, the T_{1C} value for C2,3 is 0.53 s, which is much shorter than those for the other carbons in the crystalline

region and comparable to that for the C2,3 amorphous carbon (0.53 s) (**Table S1**). The obtained relaxation value is close to a theoretical minimum value of T_{1C} (~ 0.1 s). Thus, localized molecular dynamics in a frequency close to Larmor frequency (~ 75 MHz) occurs in the *i*-hPNB crystalline region. However, such fast motions do not influence the 1 H very broadened spectra with FWHM >35 kHz. These facts indicate that fast motions occur at the C2,3 carbons of *i*-hPNB crystalline regions, however, their amplitude is very limited.

Fig. 9b shows ${}^{1}\text{H}$ - ${}^{13}\text{C}$ WISE NMR spectrum for a-hPNB at 123 ${}^{\circ}\text{C}$ above T_{cc} . The ${}^{1}\text{H}$ slice NMR spectra through all the carbons show spinning sideband patterns indicating the presence of anisotropic and large amplitude motions of a-hPNB in the crystalline region in the fast frequency regime (> 40 kHz). The minor amorphous slice also shows intense ${}^{1}\text{H}$ isotropic signals with small first SSBs (blue slice spectrum). The dynamics character for the a-hPNB chains in the crystalline regions above T_{cc} is largely different from i-hPNB above T_{cc} . These experimental facts indicate that crystal-crystal transitions differently influence chain dynamics between a- and i-hPNBs above T_{cc} .

Fig. 9c shows ¹³C CSAs of the C7 carbon for *a*-hPNB at 40 °C and 123 °C. The C7 CSA pattern is axially asymmetric at 40 °C and changes to axially symmetric one above T_{cc} , where σ_{33} is invariant and σ_{11} and σ_{22} merge. This CSA pattern can be explained in terms of molecular dynamics at the C7 site around σ_{33} axis (chain axis). Under the assumption of uniaxial diffusions, the CSA patterns were calculated under a dynamics frequency, k and depicted in **Fig. S5**. Molecular dynamics with a higher frequency >10 kHz no longer influence the ¹³C CSA line-shape (fast motional limit). The calculated CSA pattern in a frequency >10 kHz could well reproduce the experimental CSA pattern (**Fig. 9c**). Considering the well separated ¹H SSB patterns and ¹³C CSA results, it is concluded that a-hPNB conducts fast chain dynamics around the chain axis in the crystalline region in a frequency >40 kHz above T_{cc} and i- and s-hPNBs do not conduct such fast molecular dynamics up to their T_{m} s.

Two scenarios can possibly explain the axial symmetric pattern for the C7 signal. One option is uniaxial rotation of the rigid body in the crystalline region as depicted in **Fig. 7c**. Another possibility is attributed to cooperative internal C-C bond rotations with larger amplitude than those below T_{cc} as depicted in **Fig. 7d**. The T_{IC} values of all carbons in the crystalline regions are 0.7–1.6 s which are comparable to 0.35 s for C2,3 carbons in the amorphous region. These results cannot be explained in terms of rigid body model. Moreover, Register and coworkers measured that a-hPNB preserve the monoclinic lattice without lateral order and the c value goes further down to 12.1 Å in the high temperature phase. ²⁶ The contraction of the c dimension would give additional spaces for conformation dynamics of a-hPNB in the high temperature phase. All the experimental results suggest that large fluctuations of individual C-C bond rotations occur in a-hPNB crystalline region above T_{cc} .

4. Discussion

4.1. Crystallization of Configurationally Disordered *a***-hPNB.** Here, we discuss structural and dynamic origins for the unique structural evolution in *a*-hPNB during crystallization. The *a*-hPNB adopts *trans* conformation and it possesses *c* value of 12.44 Å at 23 °C. Similarly, *a*-PAN, ⁴⁶ *a*-PVA, ⁴⁷ and *a*-PVC, ⁴⁸ which show semicrystalline features, adopt *trans* conformation. Moreover, Shin *et al.* recently reported that *a*-PMMA co-crystallizes with benzoic acid (BA). ⁴⁹ It was confirmed that *a*-PMMA keeps crystalline structures after sublimation of BA. The crystallinity of *a*-PMMA is comparable to *i*- and *s*-PMMAs. It was suggested that the BA undergoes hydrogen bonding with *a*-PMMA chains and stretch *a*-PMMA chains into *trans* conformation. These existing results indicate that the extended conformation minimizes the effect of configurational disorder on the packing and thus allow even the *atacitc*-polymers to be crystallized.

Further comparisons of crystallinity of a-hPNB with those of a-PVA and a-PAN will highlight uniqueness of crystallinity of a-hPNB. Ohgi et al. systematically investigated crystallinity of PVA as a

function of stereoregularity and reported that *a*-PVA shows the minimum crystallinity of 30% among a series of stereo-regular ones. ¹⁶ Minagawa *et al.* reported crystallinity of *a*-PAN, 32–50%, the highest value of which is comparable to that of *i*-PAN. ¹⁷ However, crystallinity of *a*-PVA and *a*-PAN is much smaller than that of *a*-hPBN (82%). This indicates that only *trans*-rich conformation is not sufficient to lead to a very high crystallinity observed in *a*-hPNB. This point is further emphasized by even *i*- and *s*-hPNBs showed a lower crystallinity of 50–55% than *a*-hPNB.

Through systematic studies in the molecular dynamics of hPNBs, it is demonstrated that fast chains dynamics occurs only in a-hPNB above $T_{\rm cc}$ (115 °C). Similar fast chain dynamics have been reported in PE under high pressure and high temperature, PTFE, 11,4 trans-PBD high temperature phase, and i-PB1 form II. These polymers commonly show a very high crystallinity and a very large crystalline thickness (e.g., several μ m for ECC of PE). Considering similarity in the molecular dynamics and unique crystallization between a-hPNB and other semicrystalline polymers $^{9-11,50}$ and the absence of fast chain dynamics in s- and i-hPNBs, it is concluded that fast chain dynamics associated with the crystal-crystal transition result in the very high crystallinity and Long period in a-hPNB.

To further understand structural evolution and origins for fast chain dynamics of a-hPNB, we paid greater attention to the slow molecular dynamics of hPNBs below $T_{\rm cc}$ or $T_{\rm m}$. In *syndiotactic*-configuration, individual C-C bond rotations are frozen up to $T_{\rm m}$. Namely, the atomic positions in the cyclopentyl group are fixed up to $T_{\rm m}$ as shown in **Fig. 10**.

On the other hand, *i*-hPNB conducts small amplitude motions due to internal C-C bond rotations (conformational flexibility) above 60 °C (**Fig. 6c and 8a, b**). Above T_{cc} , the C7 carbon adopts *gauche* conformation with regarding to the C2,3 carbons in the γ position as schematically illustrated in **Fig. 9a**. This conformation change is attributed to the localized rotations around the C1-C2 (C3-C4) bonds among several bonds. **Fig. 86** depicts CODEX t_{evo} dependence of all the carbons for *i*-hPNBs at 135 °C. The decaying behavior of C2,3 is prominent and comparable to the C5,6 carbons and is much deeper

than those of the remaining carbons (C5,6 \approx C2,3 > C7 \approx C1,4). This observation is different from the CODEX decaying tendencies (C5,6 > C2,3 \approx C7 > C1,4) for a-hPNB (Fig. 7c). From the CODEX t_{evo} and non-Arrhenius behavior of the slow motions below T_{cc} as well as conformation change above T_{cc} , it is indicated that *isotactic*-configuration amplifies the local dynamics and induces steric hindrance at the C2, 3 sites above 108 °C. In DSC and ¹H NMR results, there is a large difference, $T_{\rm m}$ - $T_{\rm c}$ = 40 °C in ihPNB compared to those in s- and a-hPNBs (22 °C). This difference may arise from the conformational difference between i-hPNB and s-, a-hPNBs. The latter crystallizes in thermodynamically stable transconformation. On the other hand, trans conformation is not stable in i-hPNB above $T_{\rm cc}$. Thus, it is expected that the high-temperature phase is formed in i-hPNB when it is crystallized from the melt. Fig. **S6c** shows T_{10H} filtered ¹³C CPMAS NMR spectrum for *i*-hPNB at 25 °C, which was crystallized from the melt. The spectrum includes ¹³C signals in both low (Fig. S7a) and high temperature phases (Fig. **S7b**). This fact indicates that *i*-hPNB first crystallizes in the high temperature phase and the remaining crystallizes in the low temperature phase with further cooling. Nucleation and growth barrier for gauche conformation is lower than that for trans conformation in i-hPNB at high temperatures, however, is still high and requires a relatively low T_c of 138 °C (see Fig. 1b). It is considered that the selection of the gauche conformation during crystallization leads to a large difference in $T_{\rm m}$ - $T_{\rm c}$ for i-hPNB among three hPNBs.

a-hPNB conducts small amplitude motions around all the C-C bonds in the low temperature phase as schematically illustrated in **Fig. 10**. Temperature dependence of the dynamics follows Arrhenius line up to T_{cc} (**Fig. 8c**). This result indicates that all internal C-C bond rotations are thermally activated at all the carbon sites in the monoclinic lattice of a-hPNB. This dynamics feature is well consistent with the contraction of crystallographic c value by 0.5% between 23 and 93 °C below T_{cc} . Random configuration does not lead to the localized dynamics at the specific sites. Thermally activated C-C internal bond rotations triggers the phase transition into the high temperature phase, where the c-

dimension of a-hPNB lattice is further contracted to 12.1 Å and all carbons experience large amplitude motions in the fast frequency (>40 kHz).

By considering slow molecular dynamics in three hPNBs below T_{cc} , it is concluded that "configurational disorder coupled with conformational flexibility (CDCF)" in the low temperature phase is the origin for i) phase transition, ii) fast chain dynamics at all the carbon sites, and thus, iii) unique structural evolutions in a-hPNB. Very recently, Register and coworkers reported that T_{cc} of a-hPNB can be tuned between 134 (m:r = 52:48 and cis/trans = 100:0) and 92 °C (m:r = 52:48 and cis/trans = 78:22) by changing cis/trans configurations.⁵¹ The microstructure for the former is very similar to that for a-hPNB used in this work. At present, it is unknown why similar chemical structures give a large difference in T_{cc} . Hayano et al. reported that i- (m = 89%) and s-hPNBs (r = 70%) also show semicrystalline features.²⁹ These works further raise following questions: To what extent of stereo-irregularity and cis/trans configuration does induce unique phase transition in hPNB? How do variations in the stereoregularity and cis/trans configurations influence kinetics and geometry of molecular dynamics in cyclopentyl group of hPNBs at the atomic scale? How are molecular dynamics related to phase transition temperature and crystallization behaviors of hPNB? Further research on elaborate chemistry and physics will provide answers to the open questions in novel polyolefins.

Finally, we would like to comment on the impact of structural disorder on $T_{\rm m}$ of hPNBs. In general, $T_{\rm m}$ of semicrystalline polymer is determined by various structural factors including intermolecular interaction, packing, conformation, and lamellae thickness. All three samples possess the same chemical structure but different configurations. Therefore, intermolecular interactions do not change in all three samples. a-hPNB possessing the longest L of \sim 80 nm shows the much lower $T_{\rm m}$ = 145°C than that of i-hPNB ($T_{\rm m}$ = 178°C). The longest L value is attributed to CDCF in a-hPNB. CDCF, however, leads to less stability of the crystal and resultantly leads to the lower $T_{\rm m}$ than that of i-hPNB.

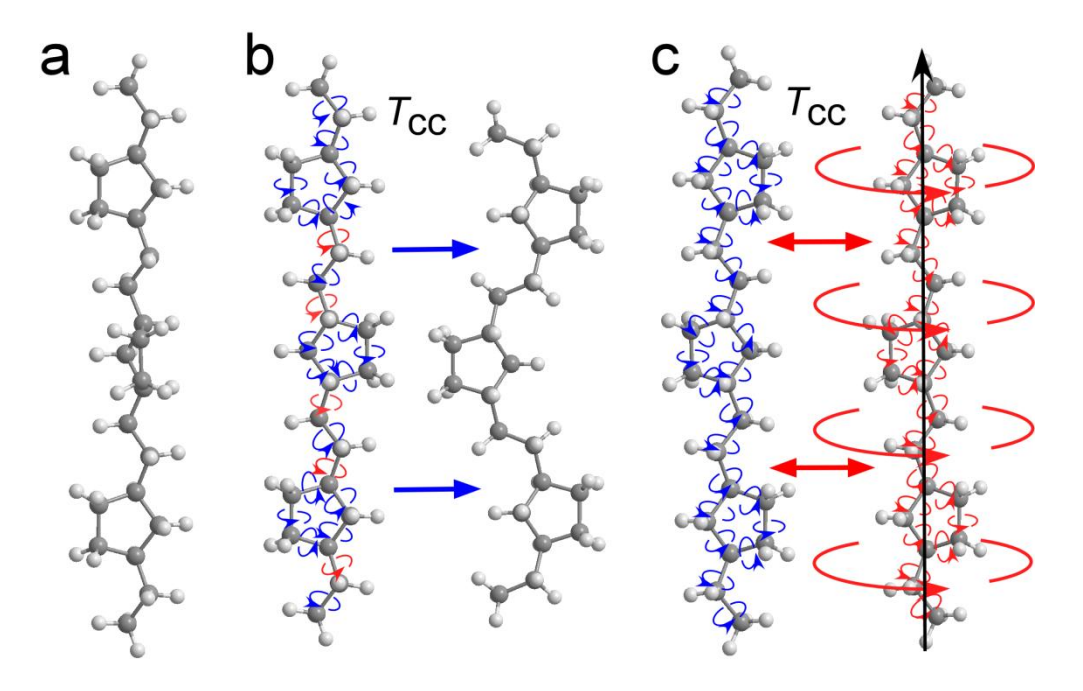


Figure 10. Schematic illustration for molecular dynamics of (a) s-, (b) i-, and (c) a-hPNBs

5. Conclusion

 atactic-hPNB. A novel concept of CDCF will be useful to design a novel semicrystalline polymer which may achieve unique structure-property relationship.

ASSOCIATED CONTENT

Supporting Information. Temperature dependence of 13 C CPMAS NMR spectra, CSA principal axis values, CODEX t_{evo} dependence of i-hPNB, CODEX spin-diffusion correction, CSA simulated pattern. "This material is available free of charge via the Internet"

AUTHOR INFORMATION

Corresponding Author

T.M. miyoshi@uakron.edu.

Author Contributions

N.K. and Y.M. equally contribute to 1st authorship. N.K., Y.M., N.Y., S.H. J.E., T.M. conceived and designed experiments. S.H. and Y.N. performed sample synthesis and SAXS experiment. N.K., Y.M., and T.M. performed ssNMR experiments. N.K. and Y.N. performed DSC experiments. N.K., Y.M., H.K. analyzed the data. All authors wrote the paper.

ACKNOWLEDGMENT

This work financially supported by NSF DMR Polymers 1708999 and 2004393.

REFERENCES

- 1) Corradini, P.; Auriemma, F.; DeRosa, C. Crystals and Crystallinity in Polymeric Materials, *Acc. Chem. Res.*, **2006**, *39*, 314-323.
- 2) Auriemma, F.; Corradini, P.; De Rosa, C. Solid Mesophases in Semicrystalline Polymers: Structural Analysis by Diffraction Techniques. *Adv. Polym. Sci.* **2005**, *181*, 1-74.
- 3) Wunderlich, B.; Grebowicz, J. Thermotropic Mesophases and Mesophase Transitions of Linear, Flexible Macromolecules. *Adv. Polym. Sci.* **1984**, *60/61*, 1-59.
- 4) Ungar, G. Thermotropic Hexagonal Phases in Polymers: Common Features and Classification. *Polymer* **1993**, *34*, 2050-2059.
- 5) Wunderlich, B.; Arakawa, T. Polyethylene Crystallized from the Melt under Elevated Pressure. *J. Polym. Sci., Part A*, **1964**, *2*, 3697-3706.

- 6) Hikosaka, M.; Amano, K.; Rastogi, S.; Keller, A. Lamellar Thickening Growth of an Extended Chain Single Crystal of Polyethylene 1. Pointers to a New Crystallization Mechanism of Polymers. *Macromolecules* **1997**, *30*, 2067-2074.
- 7) Rastogi, S.; Ungar G. Hexagonal Columnar phase in 1,4-trans-polybutadiene: morphology, chain extension, and isothermal phase reversal. *Macromolecules* **1992**, *25*, 1445-1452.
- 8) Wittman, J. C.; Smith, P.; Highly oriented thin films of poly(tetrafluoroethylene) as a substrate for oriented growth of materials. *Nature* **1991**, *352*, 414-417.
- 9) de Langen, M.; Prins, K. O. Mobility of polyethylene chains in the orthorhombic and hexagonal phases investigated by NMR. *Chem. Phys. Lett.*, **1999**, *299*, 195-200.
- 10) Moller, M. Structure and dynamics of the high-temperature polymorph of trans-1,4-polybutadiene. *Macromol. Chem. Rapid Commun.*, **1988**, *9*, 107-114.
- 11) Vega, A. J.; English, A. D. Multiple-Pulse Nuclear Magnetic Resonance of Solid Polymers. Polymer Motions in Crystalline and Amorphous Poly(tetrafluoroethylene). *Macromolecules* **1980**, *13*, 1635-1647.
- 12) Miyoshi, T.; Mamun, A.; Hu, W. Molecular Ordering and Molecular Dynamics in *Isotactic* Poly(propylene) Characterized by SS-NMR. *J. Phys. Chem. B.*, **2010**, *114*, 92-100.
- 13) Li. Z, Miyoshi, T.; Mani, S.; Koga, T.; Otsubo, A.; Kamimura, A. Solid-state NMR Characterization of the Chemical Defects and Physical Disorders in α Form of Isotactic Poly(propylene) Synthesized by Ziegler–Natta Catalysts. *Macromolecules* **2013**, *46*, 6507-6519.
- 14) Yamada, K.; Hikosaka, M.; Toda, A.; Yamazaki, S.; Tagashira, K. Equilibrium Melting Temperature of Isotactic Polypropylene with High Tacticity: 1. Determination by Differential Scanning Calorimetry. *Macromolecules* **2003**, *13*, 4790-4801.
- 15) De Rosa, C.; Auriemma, F.; de Ballesteros, O. R. A Microscopic Insight into the Deformation Behavior of Semicrystalline Polymers: The Role of Phase Transitions. *Phys. Rev. Lett.*, **2006**, *96*, 167801.
- 16) Ohgi, H.; Sato, T.; Hu, S.; Horii, F. Highly isotactic poly(vinyl alcohol) derived from tert-butyl vinyl ether. Part IV. Some physical properties, structure and hydrogen bonding of highly isotactic poly(vinyl alcohol) films. *Polymer* **2006**, *47*, 1324-1332
- 17) Minagawa, M.; Taira, T.; Yabuta, Y.; Nozaki, K.; Yoshii F. An Anomalous Tacticity-Crystallinity Relationship: A WAXD Study of Stereoregular Isotactic (83-25%) Polyacrylonitrile Powder Prepared by Urea Clathrate Polymerization. *Macromolecules* **1993**, *26*, 6903-6907.

- 18) Hobson, R. J.; Windle A. H. Crystallization and shape emulation in atactic polyvinylchoride and polyacrylonitrile. *Polymer* **1993**, *34*, 3582-3596.
- 19) Resing, H. A. NMR relaxation in adamantane and hexamethylenetetramine: Diffusion and rotation. *Mol. Cryst. Liq. Cryst.* **1969**, *9*, 101-132.
- 20) Ibberson R. M.; Telling, M. T. F.; Parsons, S. Crystal Structure and Glassy Phase Transition Behavior of Cyclohexane. *Cryst. Growth Des.*, **2008**, *8*, 512-518.
- 21) Torrisi, A.; Leech, C. K.; Shankland, K.; David, W. I. F.; Ibberson, D. R.; Beret-Buchholz, J.; Boese, R.; Leslie, M.; Catlow, C. R. A.; Price, S. L. Solid Phases of Cyclopentane: Combined Experimental and Simulation Study. *J. Phys. Chem B.*, **2008**, *112*, 3746-3758.
- 22) Mack, J. W.; Torchia, D. A. A ²H NMR Study of the Molecular Dynamics of Solid Cyclopentane. *J. Phys. Chem.*, **1991**, *95*, 4207-4213.
- 23) Tycko, R.; Dabbagh, G.; Fleming, R. M.; Haddon, R. C.; Makhjia, A. V.; Zahurak, S. M. Molecular Dynamics and The Phase Transitions in Solid C60. *Phys. Rev. Lett.*, **1991**, *67*, 1886-1889.
- 24) Robert D, J.; Costantino S, Y.; Harry C, D.; Jesse R, S.; Donald S, B. C₆₀ rotation in the solid state: Dynamics of a faceted spherical top. S*cience* **1992**, *255*, 1235-1238.
- 25) Ballesteros, O. R. d.; Cavallo, L.; Auriemma, F.; Guerra, G. Conformational analysis of poly(methylene-1,3-cyclopentane) and chain conformation in the crystalline phase. *Macromolecules* **1995**, *28*, 7355-7362.
- 26) Lee, L.-B. W.; Register, R. A. Hydrogenated Ring-Opened Polynorbornene: A Highly Crystalline Atactic Polymer. *Macromolecules* **2005**, *38*, 1216-1222.
- 27) Auriemma, F.; De Rosa, C.; Esposit, S.; Coates, G. W.; Fujita M. Crystal Structure of Alternating Isotactic Ethylene-Cyclopentene Copolymer. *Macromolecules* **2005**, *38*, 7416-7429.
- 28) Bishop, J.; Register, R. A. The Crystal-Crystal Transition in Hydrogenated Ring Opened Poly(norbornenes): Tacticity, Crystal Thickenning, and Alignment. *J. Polym. Sci., Part B: Polym. Phys.*, **2011**, *49*, 68–79.
- 29) Hayano, S.; Nakama, Y. Iso- and Syndio-Selective ROMP of Norbornene and Tetracyclododecene: Effects of Tacticity Control on the Hydrogenated Ring-Opened Poly(cycloolefin)s. *Macromolecules* **2014**, *47*, 7797-7811.
- 30) Hayano, S.; Tsunogae, Y. Syndioselective Ring-Opening Metathesis Polymerization of *endo*-Dicyclopentadiene with Tungsten Complexes Having Imido Ligands: Development of Crystalline Syndiotactic Hydrogenated Poly(*endo*-dicyclopentadiene). *Macromolecules*, **2006**, *39*, 30-38.

- 31) Hayano, S.; Kurakata, H.; Tsunogae, Y.; Nakayama, Y.; Sato, Y.; Yasuda, H. Stereospecific Ring-Opening Metathesis Polymerization of Cycloolefins Using Novel Molybdenum and Tungsten Complexes Having Biphenolate Ligands. Development of Crystalline Hydrogenated Poly(*endo*-dicyclopentadiene) and Poly(norbornene). *Macromolecules* **2003**, *36*, 7422–7431.
- 32) Liu, S. F.; Mao, J.D.; Schmidt-Rohr, K. A Robust Technique for Two-Dimensional Separation of Undistorted Chemical-Shift Anisotropy Powder Patterns in Magic-Angle-Spinning NMR. *J. Magn. Reson.*, **2002**, *155*, 15–28.
- 33) deAzevedo, E. R.; Hu, W. G.; Bonaganba, T.; Schmidt-Rohr, K. Center band-Only Detection of Exchange: Efficient Analysis of Dynamics in Solids by NMR. *J. Am. Chem. Soc.*, **1999**, *121*, 8411–8412.
- 34) Miyoshi, T.; Pascui, O.; Reichert, D. Slow chain dynamics in isotactic-poly(4–methyl–1–pentene) crystallites near the glass transition temperature characterized by solid–state C-13 MAS exchange NMR. *Macromoleucles* **2004**, *37*, 6460–6471...
- 35) Maring, D.; Meurer, B.; Weill, G. ¹H NMR studies of molecular relaxations of poly-1-butene. *J. Polym. Sci., Polym. Phys.*, **1995**, *33*, 1235–1247.
- 36) Strobl, G. The Physics of Polymers, 3rd edition, Springer-Verlag Berlin Heidelberg 2007
- 37) Hu, G. W. Boeffel, C.; Schmidt-Rohr, K. Chain Flips in Polyethylene Crystallites and Fibers Characterized by Dipolar ¹³C NMR. *Macromolecules*, **1999**, *32*, 1611–1619.
- 38) Miyoshi, T.; Hu, W.; Li, Y. Dynamic Geometry and Kinetics of Polymer Confined in Self-Assembly via Cooperative Hydrogen Bonding: A Solid state NMR Study under Paramagnetic Doping. *Macromolecules* **2010**, *43*, 4435-4437.
- 39) Schmidt-Rohr, K.; Spiess, H. W. Multidimensional Solid-State NMR and Polymers; Academic Press: London, **1994**.
- 40) Miyoshi, T.; Pascui, O.; Reichert, D. "Helical Jump Motions in Isotactic Poly(4–methyl–1–pentene) Crystallites Revealed by 1D MAS Exchange NMR Spectroscopy" *Macromolecules* **2002**, *35*, 7178–7181.
- 41) Chen, W.; Reichert. D.; Miyoshi, T. Short-Range Correlation of Successive Helical Jump Motions of Poly(L-Lactic Acid) Chains in the α Phase as Revealed by Solid-State NMR. *J. Phys. Chem. B* **2015**, *119*, 4552–4563.
- 42) Miyoshi, T.; Hayashi, S.; Imashiro, F.; Kaito, A. Chain dynamics, Conformations, and Phase Transformations for Form III Polymorph of Isotactic Poly(1–butene) Investigated by High–resolution

- Solid–state C–13 NMR Spectroscopy and Molecular Mechanics Calculations. *Macromolecules* **2002**, *35*, 2624–2632.
- 43) Pascui, O.; Beiner M.; Reichert D. Identification of Slow Dynamics Processes in Poly(n-hexyl Methacrylate) by Solid-state 1D MAS Exchange NMR. *Macromolecules* **2003**, *36*, 3992-4003.
- 44) Zemke, K.; Schmidt-Rohr, K.; Spiess, W. H. Polymer conformational structure and dynamics at the glass transition studied by multidimensional ¹³C NMR. *Acta Polym.*, **1994**, *45*, 148–159.
- 45) Abragam, A. The Principles of Nuclear Magnetism; Oxford, 1961.
- 46) Kaji, H.; Schmidt-Rohr, K. Confromation and Dynamics of Atactic Poly(acrylonitrile.1. Trans/Gauche Ratio from Double Quantum Solid-State ¹³C NMR of the Methylene Groups. *Macromolecules* **2000**, *33*, 5169–5180.
- 47) Cho, J. D.; Lyoo, W. S.; Chvalun, S. N.; Blackwell, J. X-ray Analysis and Molecular Modeling of Poly(vinyl alcohol)s with Different Stereoregularities. *Macromolecules* **1999**, *32*, 6236–6241.
- 48) Wilkes, C. E.; Flot V. F.; Krimm, S. Crystal Structure of Poly(vinyl chloride) Single Crystals. *Macromolecules* **1973**, *6*, 235–236.
- 49) Sim. J. H.; Eon, S.; Lee, S.; Oh, C.; Lee, M.; Kim, S.; Lee, W. B.; Ryu, J.; Sohn, D.; Chung, H.; Hyon, J.; Park, C.; Thomas, E. L.; Kang, Y. 1D hypo-crystals: A novel concept for the crystallization of stereo- irregular polymers. *Materials Today* **2020**, *40*, 26-37.
- 50) Miyoshi, T.; Mamun, A.; Reichert, D. "Fast Dynamics and Conformations of Polymer in a Conformational Disordered Crystal Characterized by ¹H–¹³C WISE NMR" *Macromolecules* **2010**, *43*, 3986–3989.
- 51) Klein, J. P.; Register, R. A. Tuning the Phase Behavior of Semicrystalline Hydrogenated Polynorbornene via Epimerization. *J. Polym. Sci. Polym. Phys.*, B., **2019**, 57, 1188–1195

Roles of Conformational Flexibility in the Crystallization of Stereo-irregular Polymer

Navin Kafle, Yuta Makita, Ying Zheng, Derek Schwarz, Hiromichi Kurosu, Pengju Pan, James M. Eagan, Yuki Nakama, Shigetaka Hayano, and Toshikazu Miyoshi

